Cubic or Orthorhombic? Revealing the Crystal Structure of Metastable Black-Phase $CsPbI_3$ by Theory and Experiment

Rebecca J. Sutton,[a] Marina R. Filip,[b] Amir A. Haghighirad,[c] Nobuya Sakai,[a] Bernard Wenger,[a] Feliciano Giustino,[b,d] and Henry J. Snaith*[a]

[a] Clarendon Laboratory, University of Oxford, Parks Road, Oxford OX1 3PU, United Kingdom

[b] Department of Materials, University of Oxford, Parks Road, OX1 3PH Oxford, U.K.

[c] Institut für Festkörperphysik, Karlsruhe Institute of Technology, 76021 Karlsruhe, Germany

[d] Department of Materials Science and Engineering, Cornell University, Ithaca, New York, 14853, USA

*e-mail: henry.snaith@physics.ox.ac.uk

Abstract

Room-temperature films of black-phase caesium lead iodide ($CsPbI_3$) are widely thought to be trapped in a cubic perovskite polymorph. Here, we challenge this assumption. We present structural refinement of room temperature black-phase $CsPbI_3$ in an orthorhombic polymorph. We demonstrate that this polymorph is adopted by both powders and thin-films of black-phase $CsPbI_3$, fabricated either by high- or low-temperature processes. We perform electronic band structure calculations for the orthorhombic polymorph and find agreement with experimental data and close similarities with orthorhombic methylammonium lead iodide. We investigate the structural transitions and thermodynamic stability of the various polymorphs of $CsPbI_3$, and show that the orthorhombic polymorph is the most

stable among its other perovskite polymorphs, but it remains less stable than the yellow non-perovskite polymorph.

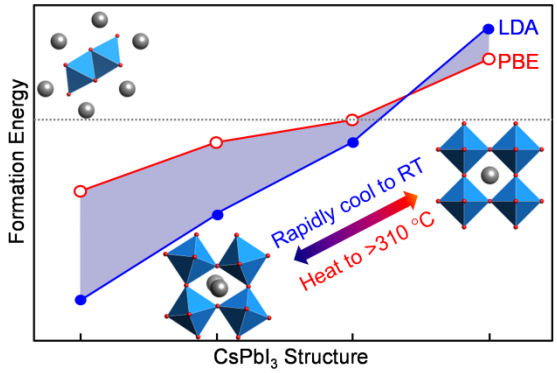

Recently there has been significant interest in the iodide-rich inorganic lead halide perovskites for optoelectronic applications. This is due to the high thermal stability of perovskites comprising an inorganic cation, in comparison to the hybrid lead-halide perovskites which comprise organic ammonium cations.[1] In particular, caesium lead iodide ($CsPbI_3$) has gained popularity due to its useful band gap of ~1.72 eV, along with the mixed halide composition $CsPbI_2Br$ which exhibits increased stability with only a small increase in band gap to ~1.92 eV.[1,2] Current best research-cell efficiencies for inorganic perovskite absorbers are around 13%, with multiple reproduced efficiencies of around 11%.[3–6]

While the inorganic perovskites are thermally stable, structurally there are significant instabilities for the iodide-rich compositions. The main hindrance to research efforts on these materials is that they readily undergo structural transitions between the desired perovskite material, thought to be a cubic perovskite, and an undesired yellow non-perovskite.[1,7] As well as being inconvenient, it is unusual for a cubic perovskite polymorph to transition directly to a non-perovskite polymorph. Additionally, measurements of the perovskite polymorph reveal no structural transitions from room temperature to 2 K for films under vacuum.[2] The absence of

any structural transitions questions the widely-held assumption that this polymorph adopts the high-temperature cubic perovskite structure.[6,8–12]

In order to overcome the structural instabilities of the iodide-rich inorganic perovskites, an accurate understanding of the structure of the perovskite polymorph is required, particularly for $CsPbI_3$. Early reports of $CsPbI_3$ proposed a 'monoclinically distorted perovskite structure', with lattice constants $a = b = 6.15$ Å, $c = 6.23$ Å, $\beta = 88.15°$, or possibly a superstructure similar to that of $CsPbBr_3$.[13,14] More recently, Stoumpos and Kanatzidis have presented tetragonal and orthorhombic structures as determined from temperature-dependent X-ray diffraction (XRD) patterns of powdered $CsPbI_3$ when slowly cooled from the cubic polymorph.[15,16] There have also been a few reports of orthorhombic structures for nanocrystals, nanowires and thin-films.[17–21]

Here, we investigate the structure of the black room-temperature polymorph of $CsPbI_3$. We isolate $CsPbI_3$ powder in a black polymorph at room temperature, for which we obtain high-quality XRD patterns. Using full refinement of these patterns, we confirm that black $CsPbI_3$ adopts an orthorhombic perovskite polymorph at room temperature which is similar to that of $CsSnI_3$. We then index XRD patterns of thin-films of $CsPbI_3$ with the orthorhombic structure, revealing strong texture in films prepared using high-temperature annealing, and weak texture for films prepared from low-temperature processing routes. We perform *GW* band structure calculations using the refined structure, and find very similar properties to the hybrid perovskites, and to experimental data, confirming that the well-studied manifestation of $CsPbI_3$ is indeed an orthorhombic perovskite. We conclude with an investigation of the structural transitions and relative stabilities by comparing the formation energies of the various polymorphs of $CsPbI_3$.

To determine the structure of room-temperature black-phase $CsPbI_3$, first we prepared a powder of $CsPbI_3$ in the yellow non-perovskite δ-$CsPbI_3$ polymorph using solid state synthesis. We ground the ingot into a powder for XRD. Comparison with the known crystal structure of the δ-$CsPbI_3$ polymorph (see Figure S1 and Table S1) verifies the product as $CsPbI_3$. Full experimental details are provided in the Supporting Information.

To obtain black-phase $CsPbI_3$ powder, we annealed the yellow δ-$CsPbI_3$ powder for approximately 20 s at 673 K until fully black, and then rapidly cooled the black powder to room temperature. We kept the powder in inert atmosphere (nitrogen gas) for repeated XRD measurements, in a sample holder with polycarbonate dome, and concluded the measurement when diffraction peaks from yellow δ-$CsPbI_3$ were visible in the XRD pattern.

We show the XRD pattern of the black powder at room temperature in Figure 1. In the XRD pattern, we observe peak splitting in the three characteristic perovskite peaks near 15°, 20° and 30° 2θ. This splitting indicates symmetry lowering from the cubic polymorph.[22] The additional reflection peaks, particularly between 20° and 30° 2θ, are suggestive of an orthorhombic structure similar to the room temperature orthorhombic $CsSnI_3$ polymorph.[23,24]

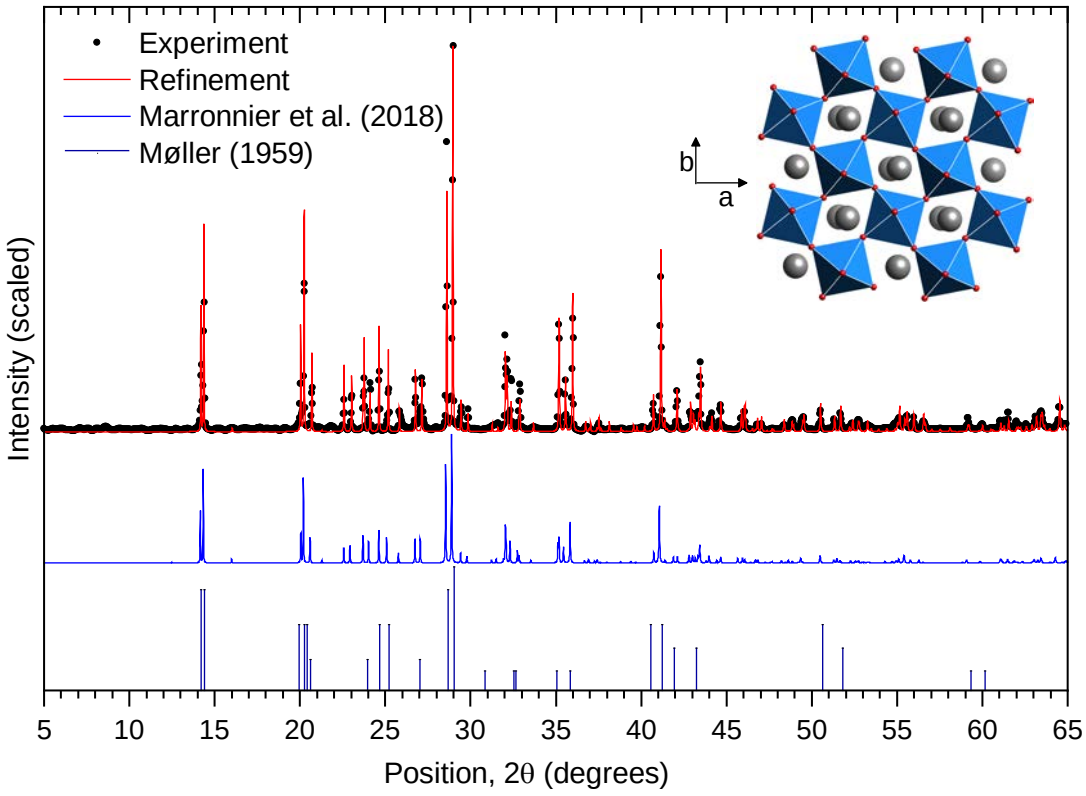

Figure 1. (black dots) XRD pattern for the black powder of γ-$CsPbI_3$ prepared by solid state synthesis, and measured with Cu $k_{\alpha 1}$ radiation at 293 K. (red line) Rietveld refinement of orthorhombic perovskite γ-$CsPbI_3$ at room temperature (polyhedral model in inset; full details provided in Table 1). (blue line) XRD pattern calculated for Cu $k_{\alpha 1}$ radiation for the orthorhombic perovskite structure determined by Marronnier et al. at 325 K.[16] *(dark blue droplines) Re-creation of the XRD pattern measured by Møller in 1959.*[13]

We performed a Rietveld refinement of the data in Figure 1. Starting from the cubic polymorph, we derived the particular orthorhombic structure for the Rietveld refinement by first principles using a sequence of tilting known as #10,[25] or $a^+b^-b^-$ in Glazer notation.[26] We show a polyhedral model of our refined structure in Figure 1 and provide our determined structural parameters in Table 1.

Recently, Marronnier *et* al. have also reported an orthorhombic polymorph of $CsPbI_3$ at 325 K.[16] In comparison, the orthorhombic structure which we have determined here exhibits subtle differences in the distortion of the octahedra which

have significant implications on the physical properties determined later in this work. Specifically, the octahedra in our structure are more elongated, with Pb–I bond lengths ranging from 3.15 to 3.22 Å (compared with 3.17 to 3.18 Å). Additionally, the octahedral tilting is greater, with β = 14.75° and δ = 9.682° (compared with 11.5° and 9.9° respectively), and the overall structure has a smaller unit cell of 947.2 Å^3 (compared to 953.9 Å^3). These structural differences are likely a result of different sample preparation methods and measurement temperature.

Originally, Møller proposed a monoclinic structure for this black polymorph.[13] We recreate the stick pattern from Møller's results in Figure 1. While the strongest lines of Møller's pattern match our experimental data, many weaker peaks are missing. This comparison strongly supports the legitimacy of the assignment of this polymorph to the orthorhombic structure.

Table 1. Summary of refined structural parameters for quench-cooled black-phase γ-$CsPbI_3$ obtained from Rietveld refinement.

Compound	$CsPbI_3$
Colour of powder	Black
Measurement temperature	293 K
Crystal system	Orthorhombic
Space group	*P n a m*
Unit cell dimensions	a = 8.8561±0.0004 Å, b = 8.5766±0.0003 Å, c = 12.4722±0.0006 Å, α = β = γ = 90°
Volume	947.33±0.05 Å^3
Z	4
Density (calculated)	5.054 g/cm^3
Number of data	2414
R_{wp}	0.07747
R_p	0.04908
Goodness of fit	1.256
Wavelength	Cu $K_{\alpha,}$ 1.540500 Å

Atomic positions

Atom	Wyckoff Position	x	y	z	Occupancy
Cs	4c	0.45995	0.50509	¼	1
Pb	4a	0	½	0	1
I	4c	0.00113	0.56202	¼	1
I	8d	0.30538	0.69731	-0.03577	1

Isotropic temperature factors, U_{iso} (Å^2)	(Cs) 0.0394 ± 0.0003, (Pb) 0.0327 ± 0.0003, (I1) 0.0385 ± 0.0004, (I2) 0.0368 ± 0.0004

For application in optoelectronic devices, it is important to determine whether the orthorhombic perovskite polymorph is also adopted by thin-films of $CsPbI_3$. Close investigation of the various reports of thin-films of $CsPbI_3$ in the literature reveals that the reported XRD patterns of black-phase $CsPbI_3$ thin-films differ between different preparation methods. Of the reports of $CsPbI_3$ thin-films in the literature, there are two contrasting preparation routes which can be grouped into high-temperature (HT) and low-temperature (LT). In the HT route, yellow non-perovskite δ-$CsPbI_3$ films are heated above the transition temperature into the black cubic α-$CsPbI_3$ perovskite polymorph and rapidly cooled. In the LT route, an additive, typically hydriodic acid (HI), is used to facilitate formation of black thin-

films at temperatures below 423 K. Here we prepare black $CsPbI_3$ thin-films and their scratched powders for analysis by XRD by both HT and LT preparation routes.

In the HT route, we prepare yellow δ-$CsPbI_3$ films by spin-coating a solution of CsI and PbI_2 in a mixed solvent containing both *N*,*N*-dimethylformamide (DMF) and dimethyl sulfoxide (DMSO).[27] To gain black films, we heat the yellow films briefly at ~620 K for approximately 2 minutes until they turn black, and then quickly cool them to room temperature under nitrogen. We present typical XRD patterns for these films in Figure 2(a). The peaks are sharp and well defined, and match well to similar XRD patterns in the literature for films prepared from vapour deposition,[27,28] or by solution-processing from DMF,[7,27,29] DMSO,[30] mixes of DMF and DMSO,[27] or even DMF with HI,[31] provided that the resulting films are annealed at temperatures above the transition to the cubic polymorph and quickly cooled. We confirm the formation of black-phase $CsPbI_3$ by absorption and steady-state photoluminescence (SSPL) of the film (see Figure S2(a)), where we see the absorption onset near 700 nm and the SSPL peak near 720 nm as expected.[1] The high temperature annealing leads to micron-sized domains (see Scanning Electron Microscope (SEM) images in Figure S2(b)), as found previously by Atomic Force Microscopy (AFM) measurements.[27]

In the LT process, we use HI as an additive in a precursor solution of CsI and PbI_2 in DMF to facilitate the formation of a black $CsPbI_3$ film at 373 K.[7] We show the XRD patterns of these films in Figure 2(c). Here we see splitting of the characteristic perovskite peaks as a shoulder at 14.2° 2θ, two peaks near 20° 2θ, and a small peak at 28.6° 2θ. This peak splitting is consistent with previous literature reports on $CsPbI_3$ prepared with HI in the precursor solution.[7,32] Similar diffraction patterns have also been found by adding BiI_3, or amines such as phenethylamine (PEA), to the precursor solution.[3,20] We provide the absorption and SSPL of our LT-processed

films in Figure S2(c). Again, the absorption onset is near 700 nm and the SSPL peak near 720 nm. In Figure S2(d) we observe polycrystalline domains of a few hundred nm across in the SEM images of the LT films, which is consistent with previous SEM and AFM measurements.[7,27]

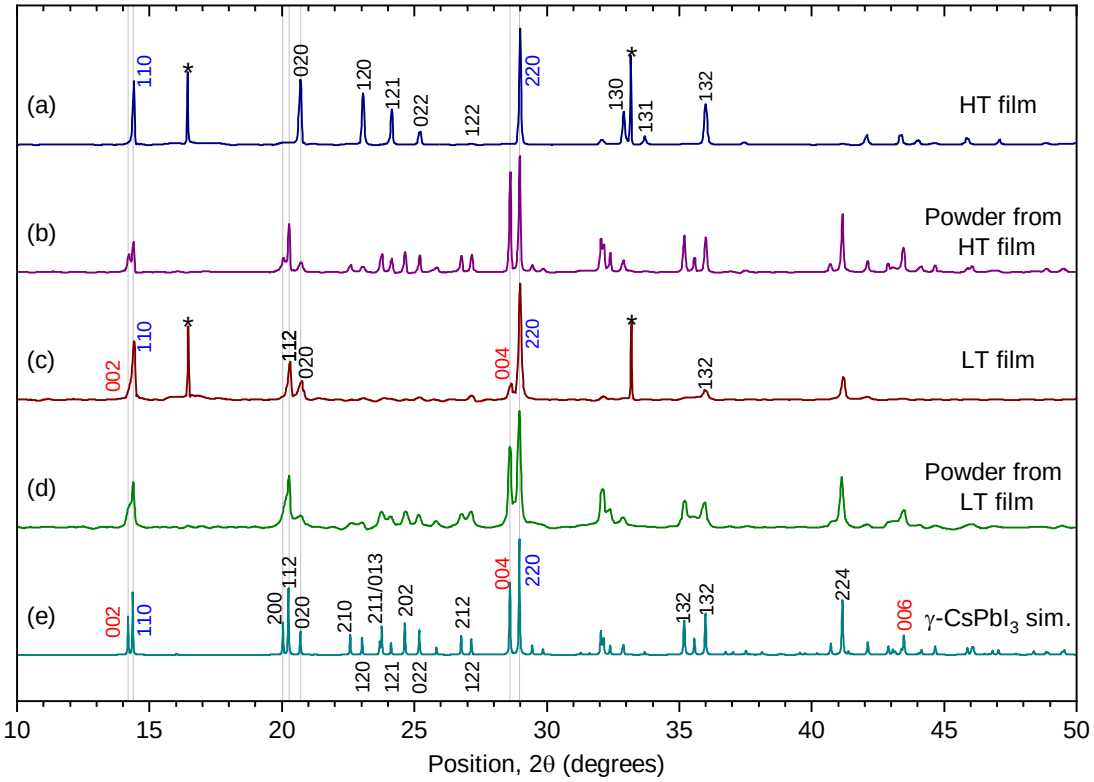

*Figure 2. XRD patterns from black γ-$CsPbI_3$ films, and powders obtained from such films, at room temperature. (a) Black films prepared by a HT route (DMF:DMSO); (b) powder scratched from the HT films. (c) Black films prepared by a LT route (DMF+HI); (d) powder scratched from the LT films. * denotes peaks from the underlying z-cut quartz substrate. All samples were prepared in nitrogen-filled domed sample holders. XRD was measured with Cu $k_{\alpha 1}$ radiation. (e) XRD pattern for our refined γ-$CsPbI_3$ orthorhombic structure, simulated and indexed using VESTA.*[33] *Miller indices are assigned for the films based on the refined pattern.*

The XRD patterns of these two films have fewer strong peaks when compared to the refined γ-$CsPbI_3$ orthorhombic structure which we presented in the previous section.

It is possible either that the films adopt a less distorted polymorph than the synthesised powder, or that some peaks are missing due to preferential orientation within the films.

To determine which of these possibilities is more likely, we scratched the films to obtain randomly oriented powders. In Figure 2(b) and (d), we show the XRD patterns for the scratched powders from the HT and LT films respectively. In both cases the peak positions align well between the films and their powders, and several additional peaks are visible in comparison to the films. Furthermore, the scratched powders both exhibit peak splitting in the three characteristic perovskite peaks near 15°, 20° and 30° 2θ. We present a reference pattern in Figure 2(e), which is the refinement of the γ-$CsPbI_3$ orthorhombic polymorph, simulated and indexed in the 3D visualization program, VESTA.[33]

Via comparison of the XRD patterns of the films and their scratched powders with the γ-$CsPbI_3$ orthorhombic polymorph, we determine that the films adopt this same orthorhombic polymorph at room temperature, but we observe preferred orientation in the films. Specifically, we find that the HT films are strongly textured, whereas the LT films are weakly textured. We assign Miller indices to the peaks in these films based on our refined γ-$CsPbI_3$ orthorhombic structure. The strongest peaks in the diffraction patterns from the films arise primarily from diffraction from the [hk0] family of planes. Orientation within the HT films is consistent with Grazing-Incidence Wide-Angle X-ray Scattering (GIWAXS) analysis of a $CsPbI_3$ film at 593 K, where crystallites within the film were determined to be oriented with the $[100]_{cubic}$ direction normal to the substrate.[34] In the γ-$CsPbI_3$ films from the HT route seen in Figure 2(a), this orientation is preserved as the film is quickly cooled, such that the strong $[100]_{cubic}$ diffraction peak becomes a strong $[110]_{orthorhombic}$ diffraction peak, and peaks from the [00l] family of planes are absent.

For the LT films fabricated with HI as an additive, in Figure 2(c) we observe an XRD pattern closer to a powder pattern but still with some preferential orientation. Unlike in the HT films, here we see peaks from the [00*l*] family of planes, although they are weaker than the 1:2 ratio expected for the [002] and [110] peaks in the γ-$CsPbI_3$ powder pattern. Intriguingly, dominant peaks from the 00*l* family of planes have been observed for LT films made using PEA as an additive where the 3D perovskite structure is retained.[20] We infer from these observations that LT additive-assisted crystallisation is able to access a different preferred orientation of the orthorhombic $CsPbI_3$ crystallites, where a significant proportion of crystallites are perpendicularly rotated through 90° in comparison with the HT processing route. We provide an illustration of these possible crystallite orientations within the films in Figure S3.

We are now able to investigate the different polymorphs of $CsPbI_3$ from *ab initio* electronic structure calculations. In Figure 3, we show the electronic band structure of γ-$CsPbI_3$ calculated within the local density approximation to density functional theory (DFT/LDA),[35,36] as implemented in the Quantum Espresso code,[37] and the *GW* approximation,[38] including spin-orbit coupling, as implemented in the Yambo code,[39] using the refined experimental crystal structure. The *GW* approximation both increases the dispersion in the valence band and shifts the conduction band rigidly when compared to the DFT/LDA eigenvalues, in close resemblance to the case of orthorhombic methylammonium lead iodide ($MAPbI_3$).[40]

We summarise the band gaps calculated for γ-$CsPbI_3$ from DFT/LDA and *GW* in Table 2. As expected, the DFT/LDA band gap is underestimated with respect to experiment by 1.2 eV. Using the *GW* approximation (see Supplementary Information), we resolve this discrepancy and obtain a band gap of 1.57 eV, 0.15 eV smaller than the experimental optical band gap of 1.72 eV at 2 K.[2] This small

discrepancy is very similar to our expected numerical error bar of 0.1 eV. Interestingly, the band gap of γ-$CsPbI_3$ is the same as we have obtained in the case of orthorhombic $MAPbI_3$ (1.57 eV).[41] We can rationalize this similarity from structural considerations. Both the experimental orthorhombic structures of $CsPbI_3$ (293 K, this work) and $MAPbI_3$ (100 K, ref 42) exhibit very similar structural features, with an average Pb-I bond length of 3.18 Å in the unit cell. In addition, the equatorial Pb-I-Pb bond angles are of 151° in both cases, while the only difference in the structure appears for the apical bond angles of 161° and 163°, for $CsPbI_3$ and $MAPbI_3$ respectively. Given this small difference in their structural features, the close similarity in the calculated *GW* band gaps of $CsPbI_3$ and $MAPbI_3$ is consistent with previous DFT predictions.[43]

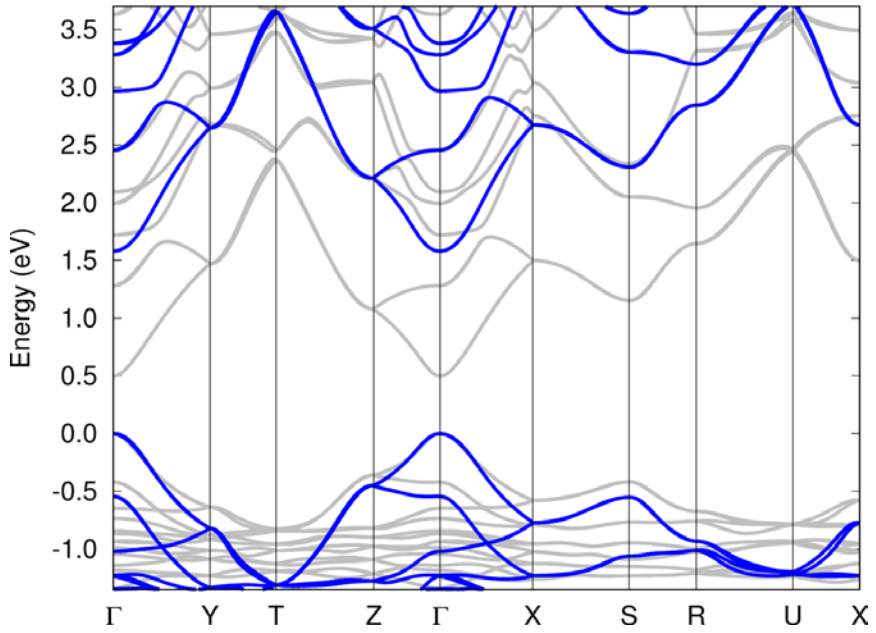

Figure 3. Comparison between the DFT/LDA (grey) and the GW (blue) band structure of the orthorhombic perovskite γ-$CsPbI_3$. The band structure is calculated on the high-symmetry path Γ [0, 0, 0] - Y [0, π/b, 0] - T [0, π/b, π/c], Z [0, 0, π/c] - Γ - X [π/a, 0, 0] - S [π/a, π/b, 0] - R [π/a, π/b, π/c] - U [π/a, 0, π/c] - X [π/a, 0, 0], where a, b and c are the lattice parameters determined experimentally in this work.

Furthermore, we note that the orthorhombic polymorph of $MAPbI_3$ is experimentally observed at temperatures below 170 K, above which there is a structural transition to the tetragonal polymorph with a corresponding change in optical band gap of at least 110 meV, when determined by the onset for the continuum in the Elliot model.[41] This difference in band gap at the structural transition is similar to the ~170 meV difference between the continuum onsets at room temperature of tetragonal $MAPbI_3$ (1.64 eV, ref [41]) and orthorhombic $CsPbI_3$ (1.81 eV, see Figure S4). These observations emphasise that the band gap in lead halide perovskites is determined primarily by the degree of octahedral tilting, and that the large difference in band gap between room temperature tetragonal $MAPbI_3$ and orthorhombic $CsPbI_3$ is governed by the difference in the structural polymorphs.

In addition, in Table 2 we show the electron and hole effective masses calculated for the orthorhombic γ-$CsPbI_3$ perovskite. As in the case of $MAPbI_3$,[40,41] we find that the electron, hole, and reduced effective masses are underestimated within DFT/LDA by almost a factor of 2, as compared to the *GW* effective masses and magneto-absorption measurements.[2] By contrast, the *GW* reduced effective mass is in excellent agreement with experiment.[2] In addition, we determine that the *GW* effective masses are very close in value for electrons and holes. This is very similar to the case of $MAPbI_3$, and consistent with experimental observation that both electrons and holes can be efficiently transported through the perovskite layer.[44]

Table 2. Band gap and effective masses calculated for orthorhombic γ-$CsPbI_3$ within DFT/LDA and GW, including spin-orbit coupling.

Method	Band gap (eV)	Electron effective mass (m_e)	Hole effective mass (m_e)	Reduced effective mass (m_e)
DFT	0.49	0.14	0.12	0.07
GW	1.57	0.23	0.24	0.12
Exp.	1.72 [2,45]	N/A	N/A	0.114±0.01 [2]

For completeness, we have also calculated the *GW* band gap for the cubic perovskite polymorph of $CsPbI_3$, which we find to be 1.14 eV (see Figure S5). From previous work, we expect that *GW* band gaps agree well with experiment for halide perovskites.[40,41,46]

To experimentally investigate the band gap of cubic α-$CsPbI_3$, we perform temperature-dependent absorption measurements on thin-films of $CsPbI_3$ (see Figures S6 and S7). We find a band gap of 1.78 eV at 623 K, which is much higher than the calculated band gap for cubic phase $CsPbI_3$ at 0 K. This difference is consistent with previous studies of the cubic phase of $MAPbI_3$, and has been associated with temperature-induced structural fluctuations of perovskites.[47–50] Both experimental and theoretical crystal structure studies conclude that the cubic structure of $MAPbI_3$ at high temperature consists of an ensemble of randomly distorted PbI_6 octahedra, and is not strictly cubic.[47–49] In a comprehensive molecular dynamics study, Ref. 51 shows that while the ensemble of these distorted structures amounts to an average cubic symmetry, at any single moment in time the average band gap of the ensemble is a larger value than that calculated for a static cubic perovskite. We expect that a similar effect takes place in the case of the cubic polymorph of $CsPbI_3$.

A recent X-ray diffraction study identified phase transitions upon slow cooling of $CsPbI_3$ from the cubic polymorph to a tetragonal polymorph at 539 K, and to the

orthorhombic polymorph at 425 K.[16] Here we probe optically if it is possible to detect associated changes in the band gap at these phase transitions. In Figure S7, we observe a continuous red-shift in the absorption onset for the $CsPbI_3$ films slowly cooled from 623 K, before conversion to the yellow δ-$CsPbI_3$ polymorph below 553 K. Within the measurement accuracy, we do not observe an abrupt change in band gap for the black polymorph over this temperature range. We also note that in previous work, the black phase of $CsPbI_3$ has been retained at temperatures right down to 2 K.[2] The main difference here is that we have cooled the perovskite film so slowly that the transition from the black to yellow polymorph is allowed, rather than being kinetically frozen in the black phase.

We now summarise diagrammatically the polymorphs of $CsPbI_3$ and their structural transitions in Figure 4(a). As previously described, the cubic polymorph α-$CsPbI_3$ has been observed by XRD to occur at high temperature, typically above 583 K and irrespective of sample history, and below the melting point above 753 K.[52,53] Slow cooling from α-$CsPbI_3$ and/or exposure to ambient moisture yields the non-perovskite δ-$CsPbI_3$,[52,53] which may also be obtained by crystal growth at room temperature.[13,14,54] This yellow polymorph differs completely from the black polymorphs in both structure and optoelectronic properties.[7]

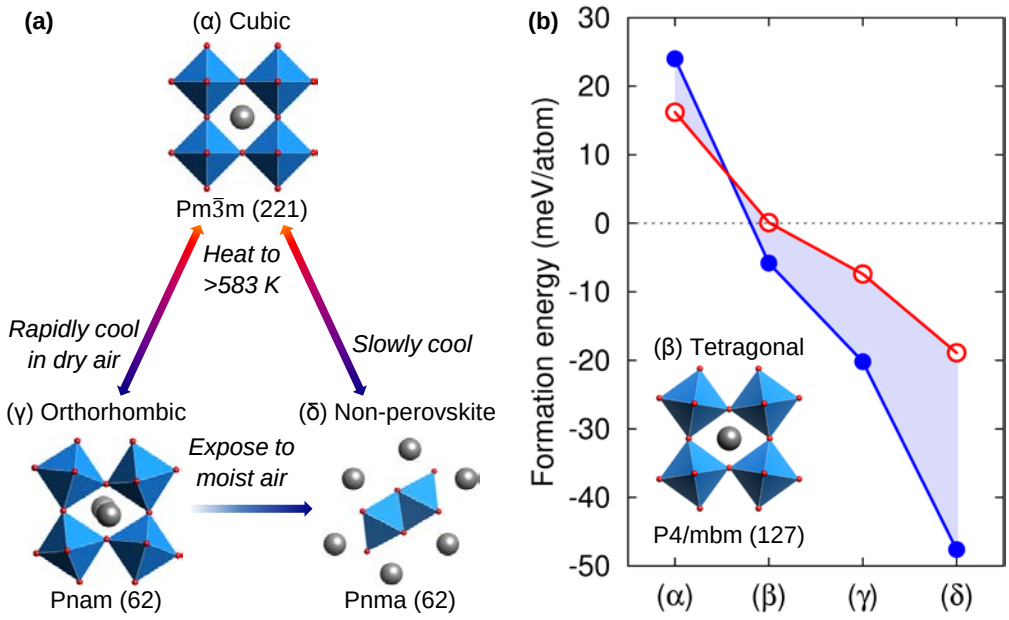

Figure 4. (a) Polyhedral models of the different polymorphs of $CsPbI_3$ and their structural transitions. Cubic α-$CsPbI_3$ occurs at temperatures above 583 K.[52,53] *Rapid cooling of α-$CsPbI_3$ in inert atmosphere yields the orthorhombic polymorph γ-$CsPbI_3$ with the structure determined in this work. δ-$CsPbI_3$ is the stable polymorph under ambient conditions.*[13,14,53,54] *(b) Formation energies calculated for the polymorphs in (a) as well as for a tetragonal β-$CsPbI_3$ polymorph simulated from β-$CsSnI_3$.*[23] *The formation energies are calculated with respect to the precursors CsI and PbI_2 as $E_f = E[CsPbI_3] - E[CsI] - E[PbI_2]$, where E is the total energy. Calculations are performed at 0 K and 0 GPa, without taking into account the effect of zero-point motion. The red circles and lines correspond to DFT/PBE calculations, while the blue dots and lines correspond to DFT/LDA calculations. The region filled in light blue highlights the difference in the formation energies calculated via the two methods.*

Here we add to this picture the orthorhombic perovskite polymorph γ-$CsPbI_3$, formed by rapid cooling of α-$CsPbI_3$ to room temperature in the absence of ambient moisture. Previously reported temperature-dependent synchrotron XRD measurements have shown that the octahedral tilting continuously increases as α-

$CsPbI_3$ is cooled, such that the structure appears to proceed through a tetragonal β-$CsPbI_3$ polymorph before reaching the γ-$CsPbI_3$ polymorph.[16] However, on heating δ-$CsPbI_3$ to the α-$CsPbI_3$ polymorph, the two polymorphs have been observed to coexist during the transition, with no orthorhombic or tetragonal polymorphs evident.[15,16,53] This coexistence means that full conversion to the α-$CsPbI_3$ polymorph, followed by rapid cooling, is always required to obtain the orthorhombic γ-$CsPbI_3$ polymorph at room temperature when starting from non-perovskite δ-$CsPbI_3$.

The thermodynamic stability of the various polymorphs of $CsPbI_3$ is of vital importance for the commercial application of this material. Here we evaluate the relative stabilities of the polymorphs by calculating their formation energies. In Figure 4(b) we show a comparison of the formation energies of the cubic, tetragonal and orthorhombic perovskite polymorphs, along with the non-perovskite polymorph. Structural information for the four polymorphs is provided in Table S2.

We calculate the formation energies within the LDA, as well as with the generalised gradient approximation (PBE) to DFT.[35] The formation energies are sensitive to the choice of exchange-correlation functional, and can differ by up to 25 meV per atom. Here we see consistent trends emerging from each functional, and so the true formation energy may be considered bracketed by the LDA and PBE values.[55] In agreement with experiment, these calculations show that the yellow polymorph is the most stable. Of the perovskite polymorphs, the most stable is the orthorhombic structure. This finding agrees with previous studies,[56] and lends weight to our argument here for the adoption of the orthorhombic polymorph by black-phase $CsPbI_3$ at room temperature. Stabilisation of the orthorhombic polymorph with respect to the cubic and tetragonal polymorphs also fits well with the relatively small tolerance factor for $CsPbI_3$, which falls between 0.81 and 0.85 (for Shannon radii)

depending on Cs coordination. In this range of tolerance factors, tilted perovskites such as the orthorhombic perovskite identified here are found to be the most stable.[57]

Notably, our experimental and theoretical investigations reveal that the instability of the black $CsPbI_3$ polymorphs with respect to the yellow polymorph constitutes an intrinsic thermodynamic property of the pure $CsPbI_3$ crystal. In addition, we propose that a robust stabilisation of all-inorganic lead-halide perovskites can be achieved by developing rational design routes to tune the total energy landscape and energy barrier for the transition between the black and yellow polymorphs through chemical substitution. Our work demonstrates that by exploring experimental investigations and predictive electronic structure calculations it may be possible to both rationalize observed stability improvements and discover candidate solutions for fully stable black inorganic lead halide perovskite polymorphs.

In this work, we have confirmed that the room temperature black polymorph of powdered samples of $CsPbI_3$ is an orthorhombic perovskite rather than a cubic perovskite. In addition, we have determined that thin-films of $CsPbI_3$, which are presently being investigated for PV and LED applications, also adopt the orthorhombic polymorph, with differences in crystallite orientation arising from different preparation methods. With the experimental structural data for the orthorhombic perovskite, we have performed calculations of the electronic band structure. The band gap and reduced effective mass show excellent agreement with experimental data, further confirming that the most commonly reported form of $CsPbI_3$ is the orthorhombic perovskite. Furthermore, we have calculated the respective formation energies of the perovskite and non-perovskite polymorphs, and found that while the orthorhombic polymorph is the most stable of the perovskite polymorphs, the non-perovskite “yellow” polymorph is the most stable overall.

These findings are in agreement with experimental data and with structural transitions in other known perovskites, and highlight the importance of octahedral tilting and distortions on the bandgap and structural stability of lead halide perovskites. These results are vital for researchers working with thin-films and powders of black $CsPbI_3$ at room temperature, and will greatly assist in the development of a structurally stable inorganic perovskite with excellent photovoltaic and optoelectronic properties.

Supporting Information

The Supporting Information is available free of charge on the ACS Publications website at DOI: XXXX

Description of experimental methods, details of calculation procedures, XRD pattern and refinement details for the non-perovskite polymorph of $CsPbI_3$, SEM, absorption and photoluminescence of $CsPbI_3$ thin films (including fitting using Elliot's model and temperature-dependent spectra), diagrams of possible crystallite orientation, electronic band structure of cubic α-$CsPbI_3$, and structural information for formation energy calculations.

Acknowledgements

R.J.S. is a Commonwealth Scholar, funded by the UK Government. This work was part funded by the Engineering and Physical Sciences Research Council (EPSRC) UK through Grants EP/M005143/1 and EP/M015254/2. B.W. acknowledges Marie Skłodowska-Curie action 706552-APPEL. M.R.F. and F.G. acknowledge the support from the Leverhulme Trust (grant RL-2012-001), the Graphene Flagship

(Horizon2020 grant no. 696656Graphene Core 1). M.R.F. and F.G. also acknowledge the use of the University of Oxford Advanced Research Computing (ARC) facility (http://dx.doi.org/10.5281/zenodo.22558), the ARCHER UK National Supercomputing Service under the "T-Dops" project, the DECI resource "Cartesius" based in The Netherlands at SURFsara and "Abel" based in Oslo with support from the PRACE AISBL, PRACE for awarding us access to MareNostrum at BSC-CNS, Spain and CSD3, UK EPSRC (Grant EP/P020259/1).

References

(1) Sutton, R. J.; Eperon, G. E.; Miranda, L.; Parrott, E. S.; Kamino, B. A.; Patel, J. B.; Hörantner, M. T.; Johnston, M. B.; Haghighirad, A. A.; Moore, D. T.; et al. Bandgap-Tunable Cesium Lead Halide Perovskites with High Thermal Stability for Efficient Solar Cells. *Adv. Energy Mater.* **2016**, *6* (8), 1502458.

(2) Yang, Z.; Surrente, A.; Galkowski, K.; Miyata, A.; Portugall, O.; Sutton, R. J.; Haghighirad, A. A.; Snaith, H. J.; Maude, D. K.; Plochocka, P.; et al. Impact of the Halide Cage on the Electronic Properties of Fully Inorganic Cesium Lead Halide Perovskites. *ACS Energy Lett.* **2017**, *2* (7), 1621–1627.

(3) Hu, Y.; Bai, F.; Liu, X.; Ji, Q.; Miao, X.; Qiu, T.; Zhang, S. Bismuth Incorporation Stabilized α-$CsPbI_3$ for Fully Inorganic Perovskite Solar Cells. *ACS Energy Lett.* **2017**, *2* (10), 2219–2227.

(4) Nam, J. K.; Chai, S. U.; Cha, W.; Choi, Y. J.; Kim, W.; Jung, M. S.; Kwon, J.; Kim, D.; Park, J. H. Potassium Incorporation for Enhanced Performance and Stability of Fully Inorganic Cesium Lead Halide Perovskite Solar Cells. *Nano Lett.* **2017**, *17* (3), 2028–2033.

(5) Bansal, S.; Chiu, M. Atmospherically Processed and Stable Cs-Pb Based Perovskite Solar Cells. *MRS Adv.* **2017**, 1–8.

(6) Swarnkar, A.; Marshall, A. R.; Sanehira, E. M.; Chernomordik, B. D.; Moore, D. T.; Christians, J. A.; Chakrabarti, T.; Luther, J. M. Quantum Dot-Induced Phase Stabilization of α-$CsPbI_3$ Perovskite for High-Efficiency Photovoltaics. *Science* **2016**, *354* (6308), 92–95.

(7) Eperon, G. E.; Paternò, G. M.; Sutton, R. J.; Zampetti, A.; Haghighirad, A. A.; Cacialli, F.; Snaith, H. J. Inorganic Caesium Lead Iodide Perovskite Solar Cells. *J. Mater. Chem. A* **2015**, *3* (39), 19688–19695.

(8) Swarnkar, A.; Mir, W. J.; Nag, A. Can B-Site Doping or Alloying Improve Thermal- and Phase-Stability of All-Inorganic $CsPbX_3$ (X = Cl, Br, I) Perovskites? *ACS Energy Lett.* **2018**, 286–289.

(9) Lau, C. F. J.; Deng, X.; Zheng, J.; Kim, J.; Zhang, Z.; Zhang, M.; Bing, J.; Wilkinson, B.; Hu, L.; Patterson, R.; et al. Enhanced Performance via Partial Lead Replacement with Calcium for a $CsPbI_3$ Perovskite Solar Cell Exceeding 13% Power Conversion Efficiency. *J. Mater. Chem. A* **2018**, *6* (14), 5580–5586.

(10) Li, B.; Zhang, Y.; Fu, L.; Yu, T.; Zhou, S.; Zhang, L.; Yin, L. Surface Passivation Engineering Strategy to Fully-Inorganic Cubic $CsPbI_3$ Perovskites for High-

Performance Solar Cells. *Nat. Commun.* **2018**, *9* (1), 1076.

(11) Lin, J.; Lai, M.; Dou, L.; Kley, C. S.; Chen, H.; Peng, F.; Sun, J.; Lu, D.; Hawks, S. A.; Xie, C.; et al. Thermochromic Halide Perovskite Solar Cells. *Nat. Mater.* **2018**, 1.

(12) Jiang, Y.; Yuan, J.; Ni, Y.; Yang, J.; Wang, Y.; Jiu, T.; Yuan, M.; Chen, J. Reduced-Dimensional α-$CsPbX_3$ Perovskites for Efficient and Stable Photovoltaics. *Joule* **2018**.

(13) Møller, C. K. Crystal Structure and Photoconductivity of Cæsium Plumbohalides. *Nature* **1958**, *182* (4647), 1436–1436.

(14) Møller, C. K. The Structure Of Cæsium Plumbo Iodide $CsPbI_3$. *Mat. Fys. Medd. Dan. Vid. Selsk.* **1959**, *32* (1), 1–18.

(15) Stoumpos, C. C.; Kanatzidis, M. G. The Renaissance of Halide Perovskites and Their Evolution as Emerging Semiconductors. *Acc. Chem. Res.* **2015**, *48* (10), 2791–2802.

(16) Marronnier, A.; Roma, G.; Boyer-Richard, S.; Pedesseau, L.; Jancu, J.-M.; Bonnassieux, Y.; Katan, C.; Stoumpos, C. C.; Kanatzidis, M. G.; Even, J. Anharmonicity and Disorder in the Black Phases of Cesium Lead Iodide Used for Stable Inorganic Perovskite Solar Cells. *ACS Nano* **2018**, *12* (4), 3477–3486.

(17) Fu, Y.; Zhu, H.; Stoumpos, C. C.; Ding, Q.; Wang, J.; Kanatzidis, M. G.; Zhu, X.; Jin, S. Broad Wavelength Tunable Robust Lasing from Single-Crystal Nanowires of Cesium Lead Halide Perovskites ($CsPbX_3$, X = Cl, Br, I). *ACS Nano* **2016**, *10* (8), 7963–7972.

(18) Lai, M.; Kong, Q.; Bischak, C. G.; Yu, Y.; Dou, L.; Eaton, S. W.; Ginsberg, N. S.; Yang, P. Structural, Optical, and Electrical Properties of Phase-Controlled Cesium Lead Iodide Nanowires. *Nano Res.* **2017**, *10* (4), 1107–1114.

(19) Paul, T.; Chatterjee, B. K.; Maiti, S.; Sarkar, S.; Besra, N.; Das, B. K.; Panigrahi, K. J.; Thakur, S.; Ghorai, U. K.; Chattopadhyay, K. K. Tunable Cathodoluminescence over the Entire Visible Window from All-Inorganic Perovskite $CsPbX_3$ 1D Architecture. *J. Mater. Chem. C* **2018**, *6* (13), 3322–3333.

(20) Fu, Y.; Rea, M. T.; Chen, J.; Morrow, D. J.; Hautzinger, M. P.; Zhao, Y.; Pan, D.; Manger, L. H.; Wright, J. C.; Goldsmith, R. H.; et al. Selective Stabilization and Photophysical Properties of Metastable Perovskite Polymorphs of $CsPbI_3$ in Thin Films. *Chem. Mater.* **2017**, *29* (19), 8385–8394.

(21) Bertolotti, F.; Protesescu, L.; Kovalenko, M. V.; Yakunin, S.; Cervellino, A.; Billinge, S. J. L.; Terban, M. W.; Pedersen, J. S.; Masciocchi, N.; Guagliardi, A. Coherent Nanotwins and Dynamic Disorder in Cesium Lead Halide Perovskite Nanocrystals. *ACS Nano* **2017**, *11* (4), 3819–3831.

(22) Linaburg, M. R.; McClure, E. T.; Majher, J. D.; Woodward, P. M. $Cs_{1-x}Rb_xPbCl_3$ and $Cs_{1-x}Rb_xPbBr_3$ Solid Solutions: Understanding Octahedral Tilting in Lead Halide Perovskites. *Chem. Mater.* **2017**, *29* (8), 3507–3514.

(23) Yamada, K.; Funabiki, S.; Horimoto, H.; Matsui, T.; Okuda, T.; Ichiba, S. Structural Phase Transitions of the Polymorphs of $CsSnI_3$ by Means of Rietveld Analysis of the X-Ray Diffraction. *Chem. Lett.* **1991**, *20* (5), 801–804.

(24) Chung, I.; Song, J.-H.; Im, J.; Androulakis, J.; Malliakas, C. D.; Li, H.; Freeman, A. J.; Kenney, J. T.; Kanatzidis, M. G. CsSnI3: Semiconductor or Metal? High Electrical Conductivity and Strong Near-Infrared Photoluminescence from a Single Material. High Hole Mobility and Phase-Transitions. *J. Am. Chem. Soc.* **2012**, *134*, 8579–8587.

(25) Woodward, P. M.; IUCr. Octahedral Tilting in Perovskites. I. Geometrical Considerations. *Acta Crystallogr. Sect. B Struct. Sci.* **1997**, *53* (1), 32–43.

(26) Glazer, A. M. The Classification of Tilted Octahedra in Perovskites. *Acta Crystallogr. Sect. B Struct. Crystallogr. Cryst. Chem.* **1972**, *28* (11), 3384–3392.

(27) Hutter, E. M.; Sutton, R. J.; Chandrashekar, S.; Abdi-Jalebi, M.; Stranks, S. D.;

Snaith, H. J.; Savenije, T. J. Vapour-Deposited Cesium Lead Iodide Perovskites: Microsecond Charge Carrier Lifetimes and Enhanced Photovoltaic Performance. *ACS Energy Lett.* **2017**, *2* (8), 1901–1908.

(28) Shahiduzzaman, M.; Yonezawa, K.; Yamamoto, K.; Ripolles, T. S.; Karakawa, M.; Kuwabara, T.; Takahashi, K.; Hayase, S.; Taima, T. Improved Reproducibility and Intercalation Control of Efficient Planar Inorganic Perovskite Solar Cells by Simple Alternate Vacuum Deposition of PbI_2 and CsI. *ACS Omega* **2017**, *2* (8), 4464–4469.

(29) Nam, J. K.; Jung, M. S.; Chai, S. U.; Choi, Y. J.; Kim, D.; Park, J. H. Unveiling the Crystal Formation of Cesium Lead Mixed-Halide Perovskites for Efficient and Stable Solar Cells. *J. Phys. Chem. Lett.* **2017**, 2936–2940.

(30) Ripolles, T. S.; Nishinaka, K.; Ogomi, Y.; Miyata, Y.; Hayase, S. Efficiency Enhancement by Changing Perovskite Crystal Phase and Adding a Charge Extraction Interlayer in Organic Amine Free-Perovskite Solar Cells Based on Cesium. *Sol. Energy Mater. Sol. Cells* **2016**, *144*, 532–536.

(31) Dastidar, S.; Hawley, C. J.; Dillon, A. D.; Gutierrez-Perez, A. D.; Spanier, J. E.; Fafarman, A. T. Quantitative Phase-Change Thermodynamics and Metastability of Perovskite-Phase Cesium Lead Iodide. *J. Phys. Chem. Lett.* **2017**, *8* (6), 1278–1282.

(32) Luo, P.; Xia, W.; Zhou, S.; Sun, L.; Cheng, J.; Xu, C.; Lu, Y. Solvent Engineering for Ambient-Air-Processed, Phase-Stable $CsPbI_3$ in Perovskite Solar Cells. *J. Phys. Chem. Lett.* **2016**, *7* (18), 3603–3608.

(33) Momma, K.; Izumi, F. VESTA: A Three-Dimensional Visualization System for Electronic and Structural Analysis. *J. Appl. Crystallogr.* **2008**, *41* (3), 653–658.

(34) Frolova, L. A.; Anokhin, D. V.; Piryazev, A. A.; Luchkin, S. Y.; Dremova, N. N.; Stevenson, K. J.; Troshin, P. A. Highly Efficient All-Inorganic Planar Heterojunction Perovskite Solar Cells Produced by Thermal Coevaporation of CsI and PbI_2. *J. Phys. Chem. Lett.* **2017**, *8* (1), 67–72.

(35) Hohenberg, P.; Kohn, W. Inhomogeneous Electron Gas. *Phys. Rev.* **1964**, *136* (3B), B864–B871.

(36) Perdew, J. P.; Zunger, A. Self-Interaction Correction to Density-Functional Approximations for Many-Electron Systems. *Phys. Rev. B* **1981**, *23* (10), 5048–5079.

(37) Giannozzi, P.; Baroni, S.; Bonini, N.; Calandra, M.; Car, R.; Cavazzoni, C.; Ceresoli, D.; Chiarotti, G. L.; Cococcioni, M.; Dabo, I.; et al. QUANTUM ESPRESSO: A Modular and Open-Source Software Project for Quantum Simulations of Materials. *J. Phys. Condens. Matter* **2009**, *21* (39), 395502.

(38) Hybertsen, M. S.; Louie, S. G. Electron Correlation in Semiconductors and Insulators: Band Gaps and Quasiparticle Energies. *Phys. Rev. B* **1986**, *34* (8), 5390–5413.

(39) Marini, A.; Hogan, C.; Grüning, M.; Varsano, D. Yambo: An Ab Initio Tool for Excited State Calculations. *Comput. Phys. Commun.* **2009**, *180* (8), 1392–1403.

(40) Filip, M. R.; Verdi, C.; Giustino, F. GW Band Structures and Carrier Effective Masses of $CH_3NH_3PbI_3$ and Hypothetical Perovskites of the Type $APbI_3$: A = NH_4, PH_4, AsH_4, and SbH_4. *J. Phys. Chem. C* **2015**, *119* (45), 25209–25219.

(41) Davies, C. L.; Filip, M. R.; Patel, J. B.; Crothers, T. W.; Verdi, C.; Wright, A. D.; Milot, R. L.; Giustino, F.; Johnston, M. B.; Herz, L. M. Bimolecular Recombination in Methylammonium Lead Triiodide Perovskite Is an Inverse Absorption Process. *Nat. Commun.* **2018**, *9* (1), 293.

(42) Baikie, T.; Fang, Y.; Kadro, J. M.; Schreyer, M.; Wei, F.; Mhaisalkar, S. G.; Graetzel, M.; White, T. J. Synthesis and Crystal Chemistry of the Hybrid Perovskite $(CH_3NH_3)PbI_3$ for Solid-State Sensitised Solar Cell Applications. *J. Mater. Chem. A* **2013**, *1* (18), 5628.

(43) Filip, M. R.; Eperon, G. E.; Snaith, H. J.; Giustino, F. Steric Engineering of Metal-

Halide Perovskites with Tunable Optical Band Gaps. *Nat. Commun.* **2014**, *5* (1), 5757.

(44) Li, F.; Ma, C.; Wang, H.; Hu, W.; Yu, W.; Sheikh, A. D.; Wu, T. Ambipolar Solution-Processed Hybrid Perovskite Phototransistors. *Nat. Commun.* **2015**, *6* (1), 8238.

(45) Eperon, G. E.; Stranks, S. D.; Menelaou, C.; Johnston, M. B.; Herz, L. M.; Snaith, H. J. Formamidinium Lead Trihalide: A Broadly Tunable Perovskite for Efficient Planar Heterojunction Solar Cells. *Energy Environ. Sci.* **2014**, *7* (3), 982.

(46) Filip, M. R.; Giustino, F. GW Quasiparticle Band Gap of the Hybrid Organic-Inorganic Perovskite CH3NH3PbI3: Effect of Spin-Orbit Interaction, Semicore Electrons, and Self-Consistency. *Phys. Rev. B* **2014**, *90* (24), 245145.

(47) Worhatch, R. J.; Kim, H.; Swainson, I. P.; Yonkeu, A. L.; Billinge, S. J. L. Study of Local Structure in Selected Organic–Inorganic Perovskites in the *Pm* $\bar{3}$ *M* Phase. *Chem. Mater.* **2008**, *20* (4), 1272–1277.

(48) Choi, J. J.; Yang, X.; Norman, Z. M.; Billinge, S. J. L.; Owen, J. S. Structure of Methylammonium Lead Iodide within Mesoporous Titanium Dioxide: Active Material in High-Performance Perovskite Solar Cells. *Nano Lett.* **2013**, *14* (1), 127–133.

(49) Weller, M. T.; Weber, O. J.; Henry, P. F.; Di Pumpo, A. M.; Hansen, T. C. Complete Structure and Cation Orientation in the Perovskite Photovoltaic Methylammonium Lead Iodide between 100 and 352 K. *Chem. Commun.* **2015**, *51* (20), 4180–4183.

(50) Zhang, Q.; Cagin, T.; Goddard, W. A. The Ferroelectric and Cubic Phases in $BaTiO_3$ Ferroelectrics Are Also Antiferroelectric. *Proc. Natl. Acad. Sci. U. S. A.* **2006**, *103* (40), 14695–14700.

(51) Quarti, C.; Mosconi, E.; Ball, J. M.; D'Innocenzo, V.; Tao, C.; Pathak, S.; Snaith, H. J.; Petrozza, A.; De Angelis, F. Structural and Optical Properties of Methylammonium Lead Iodide across the Tetragonal to Cubic Phase Transition: Implications for Perovskite Solar Cells. *Energy Environ. Sci.* **2016**, *9* (1), 155–163.

(52) Sharma, S.; Weiden, N.; Weiss, A. Phase Diagrams of Quasibinary Systems of the Type: ABX_3 — $A'BX_3$; ABX_3 — $AB'X_3$, and ABX_3 — ABX'_3; X = Halogen. *Zeitschrift für Phys. Chemie* **1992**, *175* (Part_1), 63–80.

(53) Trots, D. M.; Myagkota, S. V. High-Temperature Structural Evolution of Caesium and Rubidium Triiodoplumbates. *J. Phys. Chem. Solids* **2008**, *69* (10), 2520–2526.

(54) Wells, H. L. On the Caesium- and the Potassium-Lead Halides. *Am. J. Sci.* **1893**, *s3-45* (266), 121–134.

(55) Filip, M. R.; Liu, X.; Miglio, A.; Hautier, G.; Giustino, F. Phase Diagrams and Stability of Lead-Free Halide Double Perovskites $Cs_2BB'X_6$: B = Sb and Bi, B′ = Cu, Ag, and Au, and X = Cl, Br, and I. *J. Phys. Chem. C* **2018**, *122* (1), 158–170.

(56) Marronnier, A.; Lee, H.; Geffroy, B.; Even, J.; Bonnassieux, Y.; Roma, G. Structural Instabilities Related to Highly Anharmonic Phonons in Halide Perovskites. *J. Phys. Chem. Lett.* **2017**, 2659–2665.

(57) Woodward, P. M. Octahedral Tilting in Perovskites. II. Structure Stabilizing Forces. *Acta Crystallogr. Sect. B Struct. Sci.* **1997**, *53* (1), 44–66.